Journal of Colloid and Interface Science 356 (2011) 286–292

Contents lists available at ScienceDirect

Journal of Colloid and Interface Science

www.elsevier.com/locate/jcis

Displacement of liquid droplets on a surface by a shearing air flow

J. Fan [a], M.C.T. Wilson [b], N. Kapur [b,*]

[a] Northwestern Polytechnical University, Xi'an 710072, PR China
[b] School of Mechanical Engineering, University of Leeds, Leeds LS2 9JT, UK

ARTICLE INFO

Article history:
Received 19 July 2010
Accepted 23 December 2010
Available online 4 January 2011

Keywords:
Droplet
Shear flow
Motion
Contact line
Surface
Air flow

ABSTRACT

The motion of droplets on surfaces is crucial to the performance of a wide range of processes; this study examines the initiation of droplet motion through a shearing mechanism generated here by a controlled air flow. Systematic experiments are carried out for a range of fluids and well defined surfaces. A model is postulated that balances surface tension forces at the contact line and the drag force due to the air motion. Experiments reveal that the critical velocity at which droplet motion is initiated depends on the contact angle and the droplet size. Visualizations highlight three modes of motion: (I) the droplet retains a footprint similar to that at the point of motion; (II) a tail exists at the rear of the droplet; (III) a trail remains behind the droplet (that can shed smaller droplets). The predictions of droplet initiation velocity are good for type I motion, in accordance with the assumptions inherent within the model. This model confirms the dominant physics associated with the initiation of droplet motion and provides a useful predictive expression.

1. Introduction

The formation and motion of droplets on surfaces are important phenomena fundamental to many operations, for example in the process industries (distillation, spray coating, condensation) [1,2], agriculture (e.g. spraying of crops) [3], oil recovery [4], and in biological applications [5]. The motion of droplets can be induced by electrostatic forces (e.g. in micro-fluidic devices [6]), by temperature or chemical gradients [7,8], by shearing forces due to the motion of a surrounding fluid [9], or by the action of gravity [10–15]. It is the last case that has received the most attention, and many studies of viscous droplets sliding down inclined surfaces have been performed both experimentally [10–12] and computationally [13,14]. Key factors that affect the slide-rate are the contact angle behavior of the droplet-substrate pair, the angle of tilt of the surface, the droplet volume, and the fluid properties. For gravity-driven droplets, a number of different modes of motion have been identified including creeping, rolling and bouncing [15].

The corresponding problem, in which the liquid droplet (or gas bubble) slides along a surface due to the action of a shear flow over it, has received less attention, especially from an experimental perspective. For two fluid phases, there exist three possible combinations, which are briefly reviewed below: (i) a continuous gas phase displacing a liquid droplet; (ii) a continuous liquid phase displacing an (immiscible) liquid droplet; (iii) a continuous liquid phase displacing a gas bubble. More complex physical processes abound in nature and engineering, for example gas/liquid/liquid displacement found in the recovery of oil from porous bedrock [16], but these are beyond the scope of this review.

For liquid droplets displaced by a gas phase, Durbin [17] derived a criterion for the initiation of droplet movement by balancing the pressure due to air flow over the droplet with the surface tension forces that act to minimize droplet deformation. The air flow was modeled as inviscid and the droplets were treated as two-dimensional slender bodies. Despite these simplifications, the model demonstrated that the air velocity required to initiate droplet motion depends strongly on the contact angle hysteresis.

The displacement of a liquid droplet by a second continuous liquid phase has been studied on smooth [18] and rough [19] walls both experimentally and using a simple analytical model based on a force balance. For low Reynolds number flows, good agreement was seen between the experiments and the model for surfaces of low roughness. Theodorakakos et al. [20] investigated the detachment of a liquid drop from a porous surface under the influence of a shear flow using a computational model but with limited experimental validation. Including contact angle hysteresis within a computational model has been shown to give physically realistic droplet behavior, including droplets that leave a 'trail' [9]. Recently, Seevaratnam et al. [21] classified the type of motion of an oil droplet sliding along a hydrophobic surface in a controlled laminar water flow. They observed cases of the droplet 'sliding', 'crawling' or 'detaching', depending on the conditions of the system. Droplet detachment under cross-flow has also been studied in the context of a membrane emulsification process where spherical drops grow from the surface of a porous medium until they are swept away by a combination of shear flow and buoyancy [22,23].

* Corresponding author.
E-mail address: n.kapur@leeds.ac.uk (N. Kapur).

0021-9797/$ - see front matter © 2011 Elsevier Inc. All rights reserved.
doi:10.1016/j.jcis.2010.12.087

A set of more general theoretical models describe the two fluid phases in terms of viscosity ratio and density ratio. Consequently these cover liquid droplets being displaced by either gas or liquid, though in general the conditions are chosen to be closer to the latter. For example, Dimitrakopoulos [24] explored the deformation and onset of sliding of a droplet under a Stokes flow, and considered a wide range of viscosity ratios between the droplet and the surrounding fluid. The results demonstrate that, for such viscous dominated flows, the viscosity ratio does not affect the critical velocity of the continuous phase at which droplet motion begins, though it does influence both the rate and extent of droplet deformation under the shear flow [24,25]. Interestingly, under similar Stokes flow conditions, modeling of surfactant transport along the droplet surface has shown that surfactants tend to accumulate at the leeward side of the droplet, inducing Marangoni stresses that act to reduce droplet deformation [26]. More complex numerical models are being developed [9] which include a fuller description of the underlying physics.

Finally, the removal of gas bubbles from surfaces by a flowing continuous liquid phase finds application in systems such as gas scrubbers and in the boiling of liquids. Here the buoyancy of the bubble is a significant factor. Al-Hayes and Winterton [27] balanced the buoyancy, drag and surface tension forces and used experimental data to correct the drag coefficient to give a semi-empirical prediction of the maximum bubble diameter. More recently, Duhar and Colin [28] used a similar force balance approach but included additional terms into the expression for drag force. From a set of experiments they determined a typical value of the contact angle that the bubble makes with the surface at the point of detachment.

This paper considers, both experimentally and analytically, the initiation of liquid droplet motion on a surface, where the droplets are driven by a shearing airflow. As well as developing an analytical correlation which can be used to predict droplet movement on a surface, the extensive experimental dataset, not available elsewhere, will be of use to others working in the field.

2. Experimental method

The apparatus used in this experiment is shown schematically in Fig. 1, and features an axial fan of nominal flow rate 0.1 m^3/s with an adjustable speed controller. This draws air through a transparent polymer wind tunnel of cross-section 80 mm × 20 mm (width × height) and length 200 mm, which has a removable bottom that holds the controlled surface flush to the supporting plate. The controlled surface consisted of a microscope slide (75 mm × 25 mm) treated with one of three silanes [29] (surface A: *n*-hexyltrimethoxysilane, Sigma–Aldrich; surface B: methyltrimethoxysilane, Sigma–Aldrich; surface C: *n*-octyltriehoxysilane, Alfa Aesar) to give a range of contact angles. Prior to use, an unused microscope slide was placed in a plasma chamber (Femto, Diener electronic GmbH) for 5 min to remove any residual organic material and promote hydroxylation on the surface. The slide was then immersed in a 5% v/v mixture of silane in toluene (Fisher Scientific) and left for 1 h. After removing the slide from the solvent, it was rinsed with toluene three times and dried [30]. The slide was used within 30 min of preparation. A CCD camera (Adimec 1000c/D) and monocular microscope were positioned above the wind tunnel to capture the entire event of droplet motion at 30 frames per second, with illumination provided by a 150 W halogen light source.

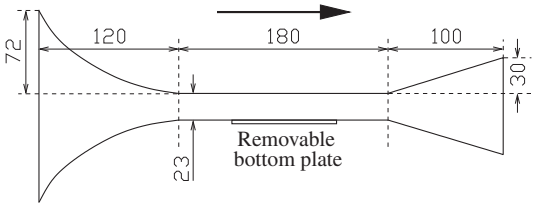

Fig. 1. Schematic of the wind tunnel used in the experiments (dimensions in mm, width 80 mm). The arrow indicates the direction of the airflow.

Recording of the droplet displacement lasted less than 30 s and was stopped after the droplet moved out of the field of view. In each experiment, a micropipette was used to position a droplet of known volume on the surface of the slide. To ensure repeatability in placement, the droplet was formed on the tip of the pipette and gently lowered onto the surface. Subsequently, the fan was started and the velocity of the air was gradually increased until the droplet motion was initiated. The previous steps were repeated three times for each set of conditions and an average velocity was obtained. In total 108 experiments were carried out.

For the droplet, three liquids were used, with composition and properties listed in Table 1. Viscosity, surface tension and density were measured using an Oswald viscometer, DuNouy ring and a density bottle, respectively, and agreed with published values. Glycerine solutions were made from fresh stock stored at 5 °C to prevent bacterial growth. Measurements of the advancing and receding contact angles were carried out for liquid 1 using a FTA 2000 where a fine capillary is used to pump fluid into or out of a droplet positioned on the surface under test. For liquids 2 and 3, a droplet was positioned on the surface under test and an inclined stage used to tilt the surface until the front of the droplet moved (giving the advancing angle) and the rear moved (giving the receding angle). In both techniques subsequent image processing was used to yield the contact angle information. The advancing and receding angles are shown in Table 2. In addition a static contact angle was measured for the droplet positioned on the slide. This angle can fall anywhere between the advancing and receding angle and is a function of the droplet deposition process itself – hence the requirement for the repeatable procedure for droplet placement described earlier. Again, image processing was used to determine this angle.

3. Results

Results are presented in terms of the air velocity required to initiate the motion of droplets of different composition and size on the range of surfaces described in Section 2. The influences of viscosity, contact angle and droplet size on this critical air speed are examined together with the corresponding shape of the droplet. An analytical model capturing the droplet behavior is described in Section 3.3.

3.1. Initiation velocity

Figs. 2–4 show graphs of the velocity required to initiate droplet motion for liquids 1–3, respectively. In all cases, as the droplet volume is increased the air velocity required to initiate motion decreases. For any given fluid and volume, those droplet-surface pairs with higher contact angles result in droplet motion at a lower air velocity. There are a number of factors that contribute to this:

Table 1
Composition and properties of the liquids used for the droplet.

Liquid	Composition	Viscosity, μ (mPa s)	Surface tension, σ (mN/m)	Density, ρ (g/ml)
1	Water	1.005	74	1.00
2	50% v/v glycerine–water	6.000	68	1.12
3	Pure glycerine	1410	63	1.26

Table 2
Contact angle measurements of droplet/surface combinations (°). Liquid 1: water; liquid 2: glycerine/water mixture; liquid 3: glycerine.

	Surface A			Surface B			Surface C		
Liquid	Static	Advan.	Rec.	Static	Advan.	Rec.	Static	Advan.	Rec.
1	90.1	99.5	76.2	85.5	87.1	60.2	80.4	82.5	48.8
2	70.5	76.4	45.9	63.7	68.2	28.7	59.1	63.7	16.1
3	54.8	59.3	24.7	53.4	58.2	19.5	50.3	54.7	10.2

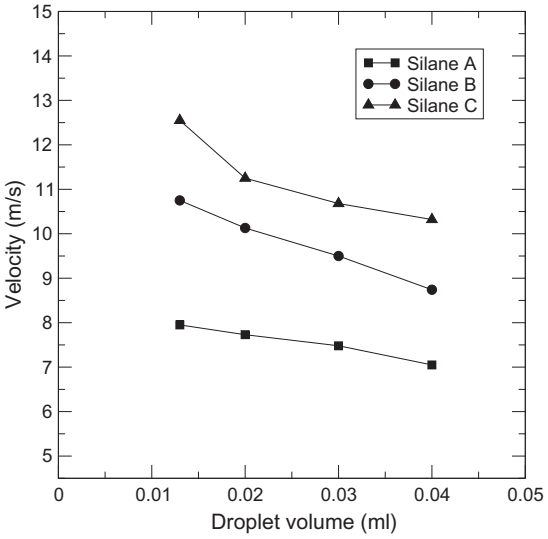

Fig. 2. Velocity required to initiate droplet motion for liquid 1 (water) on the three surfaces.

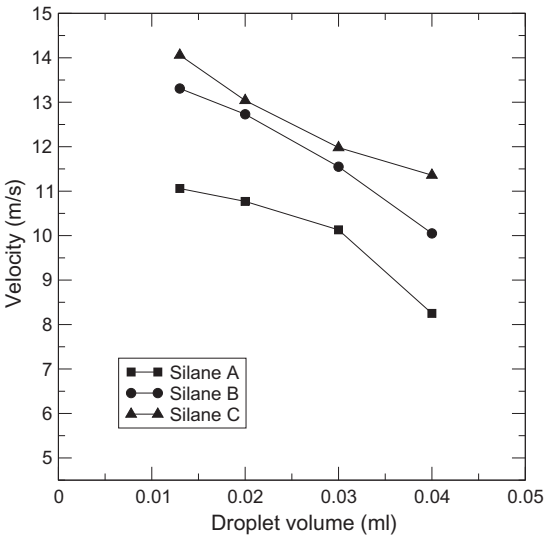

Fig. 3. Velocity required to initiate droplet motion for liquid 2 (glycerine/water) on the three surfaces.

(i) since the droplet sits within the boundary layer and experiences a velocity gradient, those drops with a higher contact angle will sit higher from the surface and see a higher mean air velocity; (ii) the force required to move the contact line will be dependent on some function of the advancing and receding angles – the simplest model of this takes the force to be proportional to $\cos\theta_R - \cos\theta_A$ [18]; (iii) the viscosity of the droplets. In previous studies [31], the terminal velocity of the sliding droplet was found by considering the balance of forces associated with pressure, viscous losses

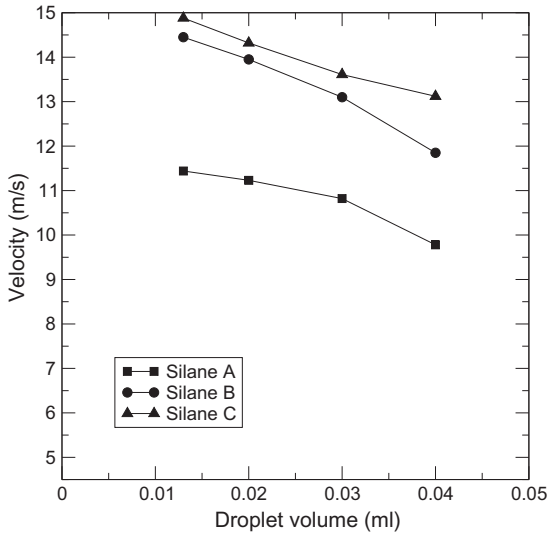

Fig. 4. Velocity required to initiate droplet motion for liquid 3 (glycerine) on the three surfaces.

within the droplet, and the contact line. Since this study is focused on initiation of droplet motion, the dependence on viscosity within the model postulated in [31] will disappear. Prior to the onset of motion, the effect of droplet viscosity will be limited to controlling the rate of deformation of the droplet surface in response to the air flow. To explore the influence of viscosity, a further set of experiments was performed using a series of Newtonian oils of viscosity 5, 10 and 20 mPa s. The controlled surface was Certonal FC732 and for all oils the advancing and receding angles were measured at 59 ± 1° and 27 ± 2° respectively.

Fig. 5 shows the air velocity needed to initiate motion (presented on the same scale as Figs. 2–4 to highlight the relative effect of viscosity). This does indeed indicate a small influence of droplet viscosity on the critical air speed, with higher viscosity droplets requiring a faster air flow. This is in contrast to analyses of Stokes flow [24,25], which show that the critical speed is independent of the droplet viscosity. However, as also discussed in those earlier works, the droplet viscosity does influence the time taken for the droplet shape to adjust in response to changes in the shear stress exerted on it. The results in Fig. 5 are consistent with the fact that less viscous droplets will deform more rapidly and hence more quickly reach a configuration beyond the equilibria permitted by contact angle hysteresis. Once this happens, the droplet will move along the surface. It should be recognized, however, that the effect of droplet viscosity on the critical air speed is significantly less than that of droplet size or contact angle. Those factors associated with droplet size and contact angles will be examined in more detail in Section 3.3.

3.2. Droplet shapes

Figs. 6–8 show the droplet shape at and just after the point of motion. A number of different scenarios emerge during the droplet

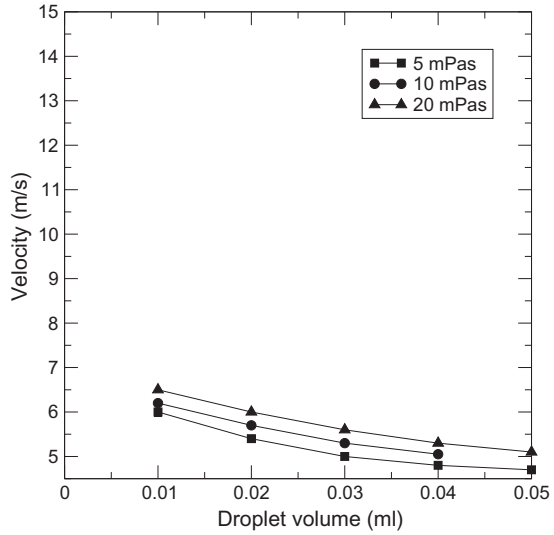

Fig. 5. Velocity required to initiate droplet motion for silicone oils on Certonal FC732 coated surface (viscosity of oil 5 mPa s, 10 mPa s, 20 mPa s).

motion. Fig. 6 shows the behavior of the water droplet on the three surfaces. In all cases the droplet footprint remains close to circular at the point of motion, but within one droplet diameter of movement, the droplet assumes an oblique back edge that is steeper than that of the original droplet. This behavior is typical of water droplets over the full range of volumes that were tested here. Only on surface C (with the lowest receding contact angle) is there any evidence of stick–slip behavior of the rear of the droplet. Fig. 7 shows the behavior of the water/glycerine mixture on the three surfaces. The advancing and receding contact angles on these surfaces are lower than those for the water case. Here there is a much stronger influence of the surface on the evolving shape of the droplet. For surface A (with the highest contact angle), the droplet remains close to its undisturbed shape at the point of motion, although the images show a contact line around the rear of the droplet that appears to move in a stick–slip manner. The droplet shape continues to evolve during the early stage of its motion,

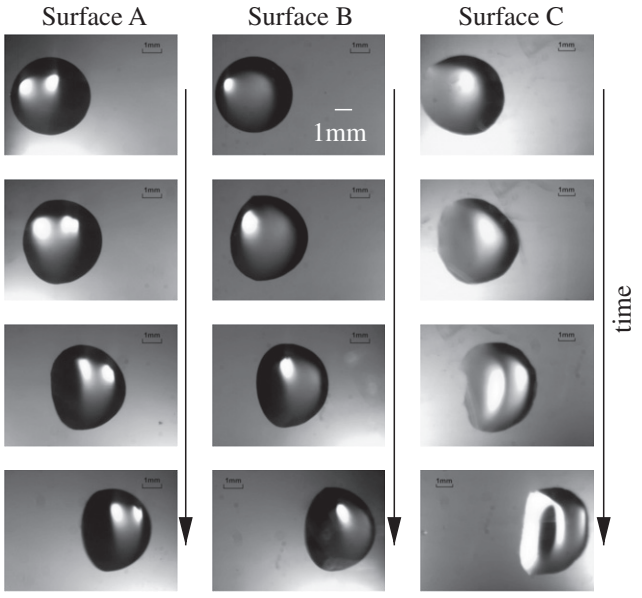

Fig. 6. Images showing a water droplet (13 μl) at and just after the point of induced motion for each of the three surfaces.

and whilst the front of the droplet is similar in shape to those of the water droplets (shown in Fig. 6), the shape of the contact line at the rear of the droplet is much closer to that seen in droplets sliding down an inclined plane [13]. However, the droplet also features the oblique ridge towards the back of the droplet observed for the water case. As the contact angle is reduced, the behavior of the rear of the droplet changes significantly. For either surfaces B or C (with much lower contact angles), the droplet leaves behind a 'trail' covering the surface. Ultimately the rear of the droplet moves at approximately the same speed as the front, and occasionally sheds small droplets, resulting in a long drawn-out droplet. Finally for the glycerine droplets (shown in Fig. 8), which give the lowest contact angles, the evolution of the droplet shape on all surfaces is similar to that observed for the glycerine/water mixture, with a more pronounced tail throughout. In terms of a qualitative comparison of the behavior between the different fluids, water on surface C shows behavior similar to glycerine/water on surface A and glycerine/water on surface C shows similar behavior to glycerine on surface A. The advancing and receding angles (Table 2) are comparable for each of these pairs, suggesting the dominance of the contact line in controlling the motion. The gross features of the behavior have been classified into three categories: (I) the droplet retains a footprint similar to that at the point of motion; (II) a tail exists at the rear of the droplet; (III) a trail remains behind the droplet (that can shed smaller droplets). This trail persists on timescales longer than that of the droplet motion, and can remain as a film on the surface. For this case, there is a corresponding reduction in size of the droplet as it moves across the surface.

3.3. Analytical model

If the contact angle hysteresis of a surface is sufficiently large, a droplet on the surface can resist the shearing action of a passing airflow in the same way that a droplet can remain pinned on an inclined surface against the action of gravity. The fact that the contact angle on the downstream side of the droplet can be larger than that on the upstream results in a capillary force, F_{CL}, acting in the upstream direction, i.e. against the airflow. This force would be proportional to $\sigma(\cos\theta_R - \cos\theta_a)$, where σ is the surface tension, if the droplet had a circular footprint and if the contact angle were θ_R everywhere on the upstream half of the droplet and θ_A everywhere on the downstream half [32].

In the case of a droplet on an incline, the maximum inclination (or minimum hysteresis) required for a pinned droplet can be found simply by balancing F_{CL} with the droplet's weight [32]. Adopting the same approach for a shear-driven droplet, the critical air speed to induce motion can be determined by balancing F_{CL} with the drag force, F_D, acting in the downstream direction due to the motion of the air over the droplet, see Fig. 9. Accounting for the directions of the forces by taking F_D as positive and F_{CL} as negative, this force balance gives

$$F_D + F_{CL} = 0 \tag{1}$$

at the point of motion. Specific forms of F_{CL} and F_D under different assumptions are given below.

A third force due to the pressure difference between the upstream and the downstream of the droplet has not been included here, with the assumption that this will be a small contribution to the overall driving force. If the droplet were to be positioned within a channel of the same order of size as the droplet (as opposed to an open flow) then this should be included [31].

To make the problem tractable from an analytical perspective, the gross geometry of the droplet at the point of motion is assumed to be that of the resting droplet, i.e. a spherical cap with height and radius determined by the static contact angle and the droplet

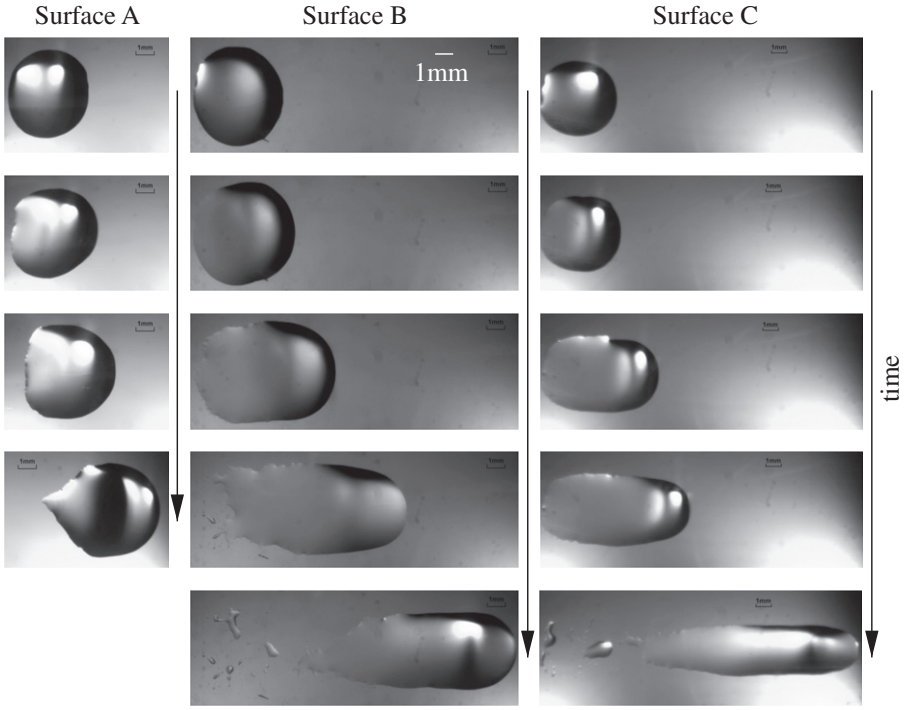

Fig. 7. Images showing a glycerine/water droplet (13 μl) at and just after the point of induced motion for each of the three surfaces.

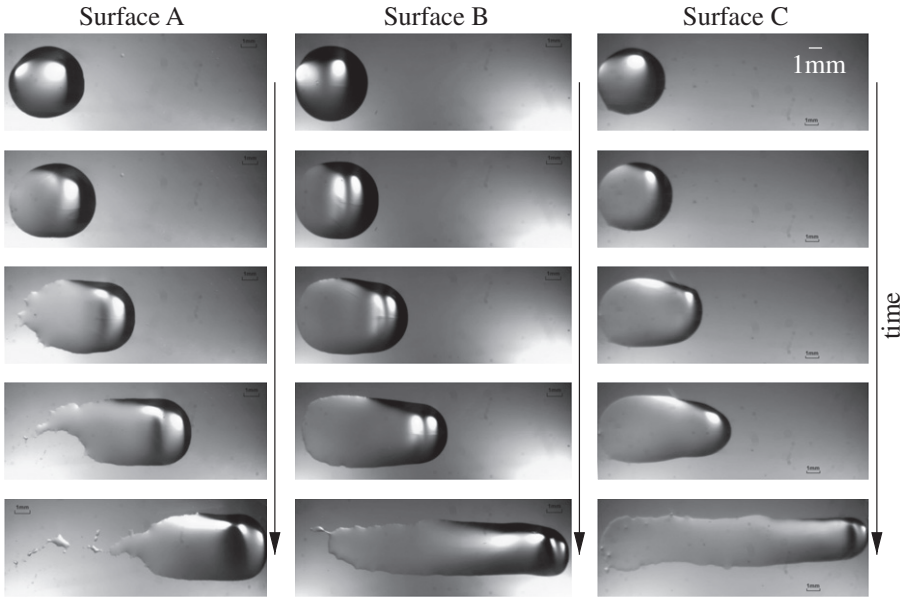

Fig. 8. Images showing a glycerine droplet (13 μl) at and just after the point of induced motion for each of the three surfaces.

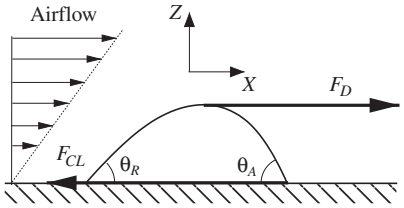

Fig. 9. Schematic showing forces on the droplet at the point when motion is initiated.

volume. In other words, it is assumed that the main shape of the droplet does not change in response to the airflow – the droplet behaves as a rigid particle would. The only deformation considered is a local variation of the contact angle around the contact line. In practice this means that the analysis will best capture the behavior of the type I droplets with dynamics such as that shown in Fig. 6.

The drag force on the droplet, F_D, is calculated by considering the flow within the laminar sub-layer and linking this to the bulk flow through the shear stress that is exerted on the surface. Previous workers, studying spherical droplets on cross flow membranes [22], relate the shear stress exerted on the droplet to the bulk using

$F = k_{x1}(6\pi R\mu V)$, which was derived earlier for a rigid spherical particle attached to a plane [33]. Here k_{x1} is a wall correction factor accounting for the proximity of the wall, R is the radius of the drop, μ is the air viscosity and V some effective velocity at the top of the droplet. For a hemispherical solid particle [34], or a hemispherical viscous droplet [35], an equivalent expression has been derived as $F = k_{x2}(6\pi R\mu V)$, where k_{x2} will be a different correction factor. Consequently the drag force exerted on the droplet, F_D, will be given by

$$F_D = k_{x2}\left(4.3\pi R_{eff}^2 \tau_w\right) \tag{2}$$

where R_{eff} is the effective radius, taken as $R_{eff} = \sqrt{H_0 R_D}$, with H_0 being the height of the droplet on the surface and R_D the radius of the interface area in contact with the surface (see Fig. 10). τ_w (taken as V/R) is the shear stress exerted on the surface of droplet. This can be estimated using a friction factor correlation [36,37]:

$$f = \frac{2\tau_w}{V_{air}^2\rho} = \begin{cases} 16/Re & Re < 500 \\ 0.0792Re^{-1/4} & Re \geqslant 500 \end{cases} \tag{3}$$

hence linking the local flow with the global air velocity. In Eq. (3), the Reynolds number is $Re = \frac{\rho V_{air} L_{eff}}{\mu}$, with $L_{eff} = 4A/S$ being a typical length scale of the flow, namely the effective diameter of the wind tunnel calculated from its cross-sectional area, A, and the perimeter of the cross-section, S. For the experiments described in Section 2, L_{eff} = 0.032 m, and a typical value of Re is 30,000. Combining these gives the force exerted on the droplet as:

$$F_D = 0.54 k_{x2} R_{eff}^2 \rho^{0.75} V_{air}^{1.75} \mu^{0.25} L_{eff}^{-0.25} \tag{4}$$

The balance of forces can be completed by considering the forces at the contact line, i.e. the capillary force arising from the contact angle hysteresis. This can be calculated by projecting the force due to surface tension onto the solid surface and integrating around the contact line. If the droplet retains its round footprint (i.e. R_D = constant) this force can be written as:

$$F_{CL} = -2\sigma R_D \int_0^{\pi} \cos\theta(\alpha)\cos\alpha d\alpha \tag{5}$$

where σ denotes the surface tension of liquid, and $\theta(\alpha)$ describes the variation in contact angle around the circular footprint, with α denoting the angular position (from $\alpha = 0$ to π and noting a symmetry plane) as shown in Fig. 10. There are a number of possibilities for describing $\theta(\alpha)$. The simplest is to assume that the front half of the droplet has contact angle θ_A and the rear θ_R. The value of F_{CL} calculated under this assumption will be denoted $F_{CLfixed}$. However, this form of $\theta(\alpha)$ implies a discontinuity in the contact angle at $\alpha = \pi/2$ and $3\pi/2$. A physically more realistic, though still simplistic, condition would be to assume a linear variation between the advancing and receding angles such that $\theta = \theta_A + \frac{\theta_R - \theta_A}{\pi}\alpha$, which will lead to a value of F_{CL} denoted by $F_{CLlinear}$. Substituting these expressions for $\theta(\alpha)$ into Eq. (5) and integrating gives:

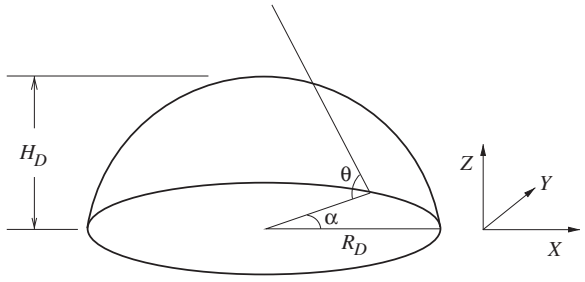

Fig. 10. Schematic showing description of the contact angle θ as a function of angular position α.

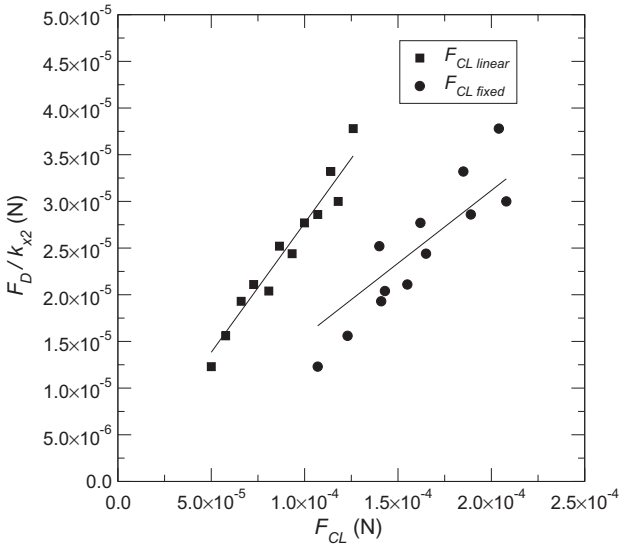

Fig. 11. Graph showing the relationship between the predicted force exerted on water droplets (Fig. 2) due to the airflow (F_D) and that to move the contact line (F_{CL}). The correction factors k_{x2} for the data are shown in Table 3.

$$F_{CLfixed} = -2\sigma R_D(\cos\theta_R - \cos\theta_A) \tag{6}$$

$$F_{CLlinear} = -\frac{2\sigma R_D \pi(\theta_A - \theta_R)(\sin(\theta_A) + \sin(\theta_R))}{-\theta_R^2 + 2\theta_R\theta_A - \theta_A^2 + \pi^2} \tag{7}$$

The ability of Eq. (1) to capture the behavior of the droplet at the start of motion is examined using the experimental data of the water droplets (Fig. 6). Fig. 11 shows a plot of the force exerted on the water droplets as a function of the force required to move the contact line, with F_D/k_{x2} calculated from Eq. (4), and $F_{CLfixed}$ and $F_{CLlinear}$ calculated from Eqs. (6) and (7) respectively. Each data point represents one experiment from Fig. 6. For the case where the linear dependence of the contact angle is assumed, there is a remarkably good correlation between F_D and $F_{CLlinear}$ (R^2 = 0.97) indicating that the analytical model contains the essential physics to capture the initiation of droplet movement for type I motion.

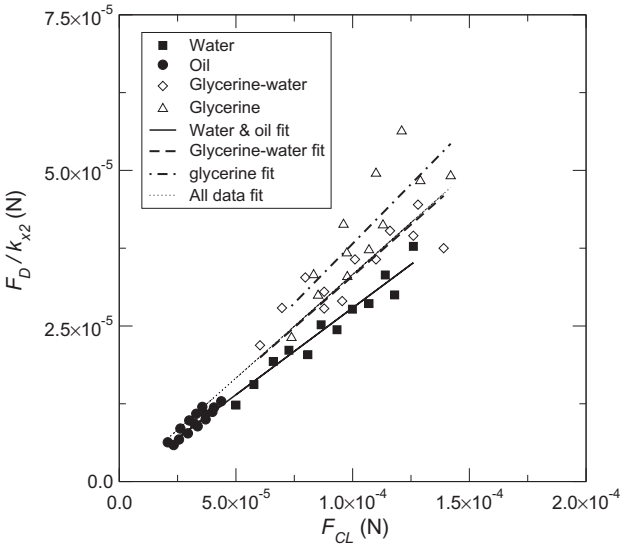

Fig. 12. Graph showing the relationship between the predicted force exerted on all droplets (Figs. 2–4) due to the airflow (F_D) and that to move the contact line ($F_{CLlinear}$) for the contact line model of linear variation of contact angle. The correction factors k_{x2} for the data are shown in Table 3.

Table 3
Values of k_{x2} and correlation coefficients for the (experimental) datasets shown in Figs. 11 and 12.

	k_{x2}	Correlation coefficient
Fig. 11		
$F_{CLlinear}$	0.28	0.97
$F_{CLfixed}$	0.16	0.91
Fig. 12		
Water and oil	0.28	0.99
Glycerine–water	0.33	0.88
Glycerine	0.38	0.85
All data	0.33	0.94

For the case where the fixed value of contact angle is assumed (giving $F_{CLfixed}$), the correlation is not as strong ($R^2 = 0.9$). This does indicate that inclusion of a realistic contact angle model is important within this modeling framework.

The same approach is extended for all the experimental data (Figs. 2–5), as shown in Fig. 12. The corresponding values for the factor k_{x2} for the datasets are shown in Table 3. The type I behavior for the water and oil data shows a high level of correlation within the framework developed here. For the type II and type III behavior the fit is less good, which is unsurprising given the complexities associated with the droplet shapes at the point of motion. Nevertheless this does give a correlation that can be used to give a reasonable estimate for the air velocity required to initiate motion. The correlation across all liquids also supports the above observation that the effect of droplet viscosity on the critical air speed is much less significant than that of the other factors.

4. Conclusions

The intricate dynamics associated with the initiation of droplet motion driven by shear flow on smooth chemically homogeneous surfaces are revealed. Features of the initial motion event have been obtained and show three modes of motion across the surface depending on the fluid and surface properties. This motion ranges from the droplets retaining a shape close to that of the original droplet during motion (type I), through droplets that have a short tail that moves at the same speed as the main droplet (type II) to droplets that leave an extensive trail that can break up under capillary forces to form smaller droplets (type III).

The associated analytical model, based on balancing the capillary forces at the contact line with the shear stress exerted from the surrounding fluid, captures the behavior of type I droplets well, in line with the assumptions inherent within the model. The simplified model of a linear variation in the contact angle around the contact line from the advancing angle to the receding angle works well for the range of contact angles examined here. The analytical framework in conjunction with the experiments shows that the contact angle hysteresis dominates the initiation of droplet movement, both in terms of the shape of the droplet and the air speed required to initiate droplet motion. The droplet viscosity has been shown to have a small influence on the critical air speed, which is not predicted by numerical or analytical work based on a Stokes flow approximation [24,25]. It would be interesting to see if similar models more appropriate to an air flow could predict this influence.

Considering the bulk shape of the droplets, a key difference between shear-driven droplets and gravity-driven droplets is the presence of the concave back and ridge-like top on the shear-driven droplets. This is a result of the droplets being 'pushed' along by the airflow acting on the surface, as opposed to being 'pulled' along by gravity acting on the bulk. This shows some similarity to the 'crawling' displacement of a liquid droplet on a hydrophobic surface by an immiscible second flowing liquid phase [21].

Finally, we make the comment that the physics of such processes are complex and associated modeling efforts must address the interdependency of the flows of air and within the droplet; in particular the complexities associated with the motion of contact lines under such scenarios remain a crucial area for research. Validation against experimental data is equally important.

Acknowledgment

Jian Fan thanks the National Natural Science Foundation of China (50976095) for providing the funding for his work.

References

[1] P. Dimitrakopoulos, J.J.L. Higdon, J. Fluid Mech. 336 (1997) 351–378.
[2] V. Cristini, Y.-C. Tan, Lab Chip 4 (2004) 257–264.
[3] D.L. Reichard, Weed Technol. 2 (1988) 82–87.
[4] J. Bear, Dynamics of Fluids in Porous Media, Dover, 1972.
[5] S.R. Hodges, O.E. Jensen, J. Fluid Mech. 460 (2002) 381–409.
[6] J. Kim, W. Shen, L. Latorre, Sens. Actuators, A 97–98 (2002) 672–679.
[7] Y.-T. Tseng, F.-G. Tseng, Sens. Actuators, A 114 (2004) 292–301.
[8] M.K. Chaudhury, G.M. Whitesides, Science 256 (5063) (1992) 1539–1541.
[9] H. Ding, P.D.M. Spelt, J. Fluid Mech. 599 (2008) 341–362.
[10] M. Sakai, A. Hashimoto, Rev. Sci. Instrum. 78 (2007) 045103.
[11] E. Rio, A. Daerr, B. Andreotti, L. Limat, Phys. Rev. Lett. 94 (2005) 024503.
[12] N. Le Grand, A. Daerr, L. Limat, J. Fluid Mech. 541 (2005) 293–315.
[13] D. Richard, D. Quéré, Europhys. Lett. 48 (3) (1999) 286–291.
[14] L.M. Pismen, Y. Pomeau, Phys. Fluids. 16 (7) (2004) 2604–2612.
[15] D. Quéré, Rep. Prog. Phys. 68 (2005) 2495–2532.
[16] I. Chatzis, A. Kantzas, F.A.L. Dullien, 1988.
[17] P.A. Durbin, J. Fluid Mech. 196 (1988) 205–222.
[18] M. Mahé, M. Vignes-Adler, A. Rouseeau, J. Colloid Interface Sci. 126 (1) (1988) 314–328.
[19] M. Mahé, M. Vignes-Adler, A. Rouseeau, J. Colloid Interface Sci. 126 (1) (1988) 329–336.
[20] A. Theodorakakos, T. Ous, M. Gavaises, J.M. Nouri, J. Colloid Interface Sci. 300 (2006) 673–687.
[21] G.K. Seevaratnam, H. Ding, O. Michel, J.Y.Y. Heng, O.K. Matar, Chem. Eng. Sci. 65 (2010) 4523–4534.
[22] S.J. Peng, R.A. Williams, Chem. Eng. Res. Des. 76 (1998) 894–901.
[23] G. De Luca, E. Drioli, J. Colloid Interface Sci. 294 (2006) 436–448.
[24] P. Dimitrakopoulos, J. Fluid Mech. 580 (2007) 451–466.
[25] E.B. Dussan V, J. Fluid Mech. 174 (1987) 381–397.
[26] A.D. Schleizer, R.T. Bonnecaze, J. Fluid Mech. 383 (1999) 29–54.
[27] A.M. Al-Hayes, R.H.S. Winterton, Int. J. Heat Mass Transfer 24 (1981) 223–230.
[28] G. Duhar, C. Colin, Phys. Fluids 18 (2006) 077101.
[29] T. Kawakatsu, G. Trägårdh, Ch. Trägårdh, M. Nakajima, N. Oda, T. Yonemoto, Colloids Surf., A 179 (2001) 29–37.
[30] J.J. Cras, C.A. Rowe-Taitt, D.A. Nivens, F.S. Ligler, Biosens. Bioelectron. 14 (1999) 683–688.
[31] L. Hao, P. Cheng, Int. J. Heat Mass Transfer 53 (2010) 1243–1246.
[32] D. Quéré, M.-J. Azzopardi, L. Delattre, Langmuir 14 (1998) 2213–2216.
[33] M.E. O'Neill, Chem. Eng. Sci. 23 (1968) 1293–1298.
[34] T.C. Price, Q. J. Mech. Appl. Math. 38 (1985) 93–104.
[35] K. Sugiyama, M. Sbragaglia, J. Eng. Math. 62 (2008) 35–50.
[36] R.B. Bird, W.E. Stewart, E.N. Lightfoot, Transport Phenomena, Wiley, New York, 1960.
[37] P.R.H. Blasius, Das Aehnlichkeitsgesetz bei Reibungsvorgangen in. Flüssigkeiten. Forschungsheft 131 (1913) 1–41.